protein C activity in the general population of Japan; women with the GG genotype exhibit approximately 5% higher plasma protein C activity ($p=0.002$) than those with either the GA or AA genotypes [20]. The R325Q mutation is predicted by the topological model to reside within the cytoplasmic domain of GGCX [24]. In this domain, amino acids 343–355 mediate GGCX enzyme/substrate interactions; residues 343–345 of CVY are necessary for both substrate binding and γ-carboxylase activity [25].

Recent studies reported the association of a microsatellite marker in intron 6 of *GGCX* with warfarin dose [26,27]. In 45 warfarin-treated Japanese patients, 10, 11, and 13 CAA repeats were detected. Three individuals heterozygous for the 13 repeat allele required higher maintenance doses than patients with fewer repeats [26]. In 183 warfarin-treated Swedes, a group of individuals bearing both alleles with 13 repeats or those with 14–16 repeats required significantly higher maintenance doses than patients with fewer repeats. Taken together, GGCX is a promising candidate influencing warfarin maintenance doses significantly. Further studies with larger populations and additional ethnic groups are required to elucidate the association between variations in warfarin dosages and the *GGCX* 8016G>A genotype.

Acknowledgments

This study was supported by the Program for the Promotion of Fundamental Studies in Health Sciences of the National Institute of Biomedical Innovation (NIBIO), a Grant-in-Aid from the Ministry of Health, Labor, and Welfare of Japan, and the Ministry of Education, Culture, Sports, Science, and Technology of Japan. We thank Ms. Junko Ishikawa for her technical assistance.

References

[1] Rost S, Fregin A, Ivaskevicius V, Conzelmann E, Hortnagel K, Pelz HJ, et al. *VKORC1* cause warfarin resistance and multiple coagulation factor deficiency type 2. *Nature* 2004;**427**:537–41.

[2] Li T, Chang CY, Jin DY, Lin PJ, Khvorova A, Stafford DW. Identification of the gene for vitamin K epoxide reductase. *Nature* 2004;**427**:541–4.

[3] Wajih N, Sane DC, Hutson SM, Wallin R. The inhibitory effect of calumenin on the vitamin K-dependent γ-carboxylation system. Characterization of the system in normal and warfarin-resistant rats. *J Biol Chem* 2004;**279**:25276–83.

[4] D'Andrea G, D'Ambrosio RL, Di Perna P, Chetta M, Santacroce R, Brancaccio V, et al. A polymorphism in the *VKORC1* gene is associated with an interindividual variability in the dose-anticoagulant effect of warfarin. *Blood* 2005;**105**:645–59.

[5] Bodin L, Verstuyft C, Tregouet DA, Robert A, Dubert L, Funck-Brentano C, et al. Cytochrome P450 2C9 *(CYP2C9)* and vitamin K epoxide reductase *(VKORC1)* genotypes as determinants of acenocoumarol sensitivity. *Blood* 2005;**106**: 135–40.

[6] Rieder MJ, Reiner AP, Gage BF, Nickerson DA, Eby CS, McLeod HL, et al. Effect of *VKORC1* haplotypes on transcriptional regulation and warfarin dose. *N Engl J Med* 2005;**352**:2285–93.

[7] Yuan HY, Chen JJ, Lee MT, Wung JC, Chen YF, Charng MJ, et al. A novel functional VKORC1 promoter polymorphism is associated with inter-individual and inter-ethnic differences in warfarin sensitivity. *Hum Mol Genet* 2005;**14**: 1745–51.

[8] Sconce EA, Khan TI, Wynne HA, Avery P, Monkhouse L, King BP, et al. The impact of *CYP2C9* and *VKORC1* genetic polymorphism and patient characteristics upon warfarin dose requirements: proposal for a new dosing regimen. *Blood* 2005;**106**:2329–33.

[9] Veenstra DL, You JH, Rieder MJ, Farin FM, Wilkerson HW, Blough DK, et al. Association of Vitamin K epoxide reductase complex 1 *(VKORC1)* variants with warfarin dose in a Hong Kong Chinese patient population. *Pharmacogenet Genomics* 2005;**15**:687–91.

[10] Wadelius M, Chen LY, Downes K, Ghori J, Hunt S, Eriksson N, et al. VKORC1 and GGCX polymorphisms associated with warfarin dose. *Pharmacogenomics J* 2005;**5**:262–70.

[11] Takahashi H, Wilkinson GR, Nutescu EA, Morita T, Ritchie MD, Scordo MG, et al. Different contributions of polymorphisms in VKORC1 and CYP2C9 to intra- and inter-population differences in maintenance dose of warfarin in Japanese, Caucasians and African-Americans. *Pharmacogenet Genomics* 2006;**16**:101–10.

[12] Vecsler M, Loebstein R, Almog S, Kurnik D, Goldman B, Halkin H, et al. Combined genetic profiles of components and regulators of the vitamin K-dependent γ-carboxylation system affect individual sensitivity to warfarin. *Thromb Haemost* 2006;**95**:205–11.

[13] Mushiroda T, Ohnishi Y, Saito S, Takahashi A, Kikuchi Y, Saito S, et al. Association of *VKORC1* and *CYP2C9* polymorphisms with warfarin dose requirements in Japanese patients. *J Hum Genet* 2006;**51**:249–53.

[14] Lee SC, Ng SS, Oldenburg J, Chong PY, Rost S, Guo JY, et al. Interethnic variability of warfarin maintenance requirement is explained by *VKORC1* genotype in an Asian population. *Clin Pharmacol Ther* 2006;**79**:197–205.

[15] Montes R, Ruiz de Gaona E, Martinez-Gonzalez MA, Alberca I, Hermida J. The c.−1639G>A polymorphism of the *VKORC1* gene is a major determinant of the response to acenocoumarol in anticoagulated patients. *Br J Haematol* 2006;**133**: 183–7.

[16] Higashi MK, Veenstra DL, Kondo LM, Wittkowsky AK, Srinouanprachanh SL, Farin FM, et al. Association between *CYP2C9* genetic variants and anticoagulation-related outcomes during warfarin therapy. *JAMA* 2002; **287**:1690–8.

[17] Nasu K, Kubota T, Ishizaki T. Genetic analysis of *CYP2C9* polymorphism in a Japanese population. *Pharmacogenetics* 1997;**7**:405–9.

[18] Yamaguchi T. Optimal intensity of warfarin therapy for secondary prevention of stroke in patients with nonvalvular atrial fibrillation: a multicenter, prospective, randomized trial. Japanese Nonvalvular Atrial Fibrillation-Embolism Secondary Prevention Cooperative Study Group. *Stroke* 2000;**31**:817–21.

[19] Chimowitz MI, Lynn MJ, Howlett-Smith H, Stern BJ, Hertzberg VS, Frankel MR, et al. Comparison of warfarin and aspirin for symptomatic intracranial arterial stenosis. *N Engl J Med* 2005;**352**:1305–16.

[20] Kimura R, Kokubo Y, Miyashita K, Otsubo R, Nagatsuka K, Otsuki T, et al. Polymorphisms in vitamin K-dependent

γ-carboxylation-related genes influence interindividual variability in plasma protein C and protein S activity in general population. Int J Hematol in press.

[21] Antonarakis SE. Recommendations for a nomenclature system for human gene mutations. Nomenclature Working Group. *Hum Mutat* 1998;**11**:1–3.

[22] Tanaka C, Kamide K, Takiuchi S, Miwa Y, Yoshii M, Kawano Y, et al. An alternative fast and convenient genotyping method for the screening of angiotensin converting enzyme gene polymorphisms. *Hypertens Res* 2003;**26**:301–6.

[23] Sanderson S, Emery J, Higgins J. *CYP2C9* gene variants, drug dose, and bleeding risk in warfarin-treated patients: a HuGEnet systematic review and meta-analysis. *Genet Med* 2005;**7**:97–104.

[24] Tie J, Wu SM, Jin D, Nicchitta CV, Stafford DW. A topological study of the human γ-glutamyl carboxylase. *Blood* 2000;**96**:973–8.

[25] Pudota BN, Hommema EL, Hallgren KW, McNally BA, Lee S, Berkner KL. Identification of sequences within the γ-carboxylase that represent a novel contact site with vitamin K-dependent proteins and that are required for activity. *J Biol Chem* 2001;**276**:46878–86.

[26] Shikata E, Ieiri I, Ishiguro S, Aono H, Inoue K, Koide T, et al. Association of pharmacokinetic *(CYP2C9)* and pharmacodynamic (*factors II, VII, IX,* and *X*; *proteins S* and *C*; and *γ-glutamyl carboxylase*) gene variants with warfarin sensitivity. *Blood* 2004;**103**:2630–5.

[27] Chen LY, Eriksson N, Gwilliam R, Bentley D, Deloukas P, Wadelius M. γ-Glutamyl carboxylase (GGCX) microsatellite and warfarin dosing. *Blood* 2005;**106**:3673–4.

[28] Sullivan-Klose TH, Ghanayem BI, Bell DA, Zhang ZY, Kaminsky LS, Shenfield GM, et al. The role of the CYP2C9-Leu359 allelic variant in the tolbutamide polymorphism. *Pharmacogenetics* 1996;**6**:341–9.

AJH 2006; 19:403–406

Primary Intracerebral Hemorrhage During Asleep Period

Yoshinari Nagakane, Kotaro Miyashita,
Kazuyuki Nagatsuka, Takemori Yamawaki, and Hiroaki Naritomi

Background: The onset of intracerebral hemorrhage (ICH) has a circadian variation, with a lower risk during the asleep period. It is unclear, however, whether ICH during the asleep period differs from that during the awake period in pathophysiologic nature. The purpose of this study is to elucidate the incidences and clinical features of ICH during the asleep period.

Methods: We studied 129 consecutive patients with primary ICH and classified them into two groups according to the circumstance of their stroke onset, either during the awake period (awake ICH group) or the asleep period (asleep ICH group). Demographic and clinical characteristics were then compared between the two groups.

Results: Of the patients, 19 (14.7%) had ICH during the asleep period. The mortality rate at 1 month after the stroke was significantly higher in the asleep ICH group than in the awake ICH group (21.1% *v* 4.9%, $P = .0325$). The hemorrhage volume in the asleep ICH group was also significantly larger than that in the awake ICH group (mean volume, 32.6 mL *v* 16.7 mL, $P = .0122$).

Conclusions: Our findings indicate that ICH during the asleep period may be more detrimental compared with ICH during the awake period, causing larger hematoma and higher mortality rates. Am J Hypertens 2006;19: 403–406 © 2006 American Journal of Hypertension, Ltd.

Key Words: Blood pressure, circadian rhythm, intracerebral hemorrhage, sleep apnea syndromes, stroke onset.

The onset of stroke has a specific circadian variation. It is generally considered that intracerebral hemorrhage (ICH) during the asleep period is extremely rare[1] because of the lower blood pressure (BP) levels at night.[2,3] Many neurologists also consider that ICH during the asleep period may be smaller, as the lower BP circumstance is unlikely to increase the size of hematoma.[4] However, no study to date has focused on the clinical features of ICH during the asleep period. The present study was undertaken to elucidate the incidence and clinical features of ICH during the asleep period.

Methods

Between January 1, 1996, and December 31, 2000, a total of 157 consecutive patients with acute nontraumatic ICH were admitted to our department. The diagnosis of ICH was established on the basis of CT findings, which were obtained within 60 min after the patients' arrival in all cases. Of the patients, 28 patients were excluded from the present study because the hemorrhage was related to ruptured aneurysms, vascular malformations, brain tumors, brain infections, anticoagulation, hematologic abnormalities, or amyloid angiopathy. The study was carried out in the remaining 129 patients, all of whom had primary ICH.

Hematoma volumes were measured with the ABC/2 formula, in which where A is the largest diameter of the hematoma, B is the largest diameter of the hematoma perpendicular to A on the same slice, and C is the number of slices showing hematoma multiplied by the slice thicknessis, as described in Kothari et al.[5] The size of hematoma was classified into two grades: large (based on a hematoma volume of ≥30 mL) and small (hematoma volume of <30 mL). Clinical outcome was assessed using the modified Rankin scale score and the mortality rate at 1 month after the stroke. The information concerning the onset of stroke, during either the awake period or asleep period, was obtained from the patients themselves or from others who witnessed the patients' stroke episodes.

The patients were divided into two groups according to the onset time of ictus. The first group comprised patients

Received July 25, 2005. First decision October 20, 2005. Accepted October 20, 2005.

From the Department of Cerebrovascular Medicine (YN, KM, KN, TY, HN), National Cardiovascular Center, Osaka, Japan; and Department of Neurology (YN), Research Institute for Neurological Diseases and Geriatrics, Kyoto Prefectural University of Medicine, Kyoto, Japan.

Address correspondence and reprint requests to Dr. Yoshinari Nagakane, Department of Neurology, Research Institute for Neurological Diseases and Geriatrics, Kyoto Prefectural University of Medicine, 465 Kajii-cho, Kamigyo-ku, Kyoto 602-8566, Japan; e-mail: nagakane@koto.kpu-m.ac.jp

0895-7061/06/$32.00
doi:10.1016/j.amjhyper.2005.10.013

developed ICH during the asleep period (asleep ICH group), and the other comprised patients who developed ICH during the awake period (awake ICH group). The patients who first noticed their symptoms upon awakening or those who were found unconscious in bed when family members tried to wake them up were included into the asleep ICH group. The demographic and clinical characteristics were then compared between the two groups.

Data was statistically analyzed using the Fisher exact test or χ^2 test for proportions. The Mann-Whitney test was used for nonparametric variables, and the unpaired t test was used for normal variables.

Results

The demographic and clinical characteristics of the patients are shown in Table 1. Of the 129 patients, 19 (14.7%) had ICH during the asleep period, and 103 (79.8%) had ICH during the awake period. The remaining seven patients (5.4%) could not be categorized in either group, as the information concerning the onset of their strokes was not available for these patients. In the asleep ICH group, two patients were found unconscious in bed the morning after their ICH when family members tried to wake them up; seven were observed by family members to have stertorous respirations or unusual vocalizations in the middle of the night, and the remaining patients noticed their symptoms upon awakening the next morning. However, there were no significant differences in the baseline variables between these two groups. All 19 patients in the asleep ICH group had a history of hypertension. Of these 19 patients, 12 were taking antihypertensive medication before the occurrence of ICH, whereas six were not receiving any antihypertensive medication, and the remainder had no available information concerning their recent BP control. The mortality rate at 1 month after the stroke was significantly higher in the asleep ICH group (4/19, 21.1%) than in the awake ICH group (5/103, 4.9%) ($P = .0325$).

Parenchymal hematoma volumes, which were calculated from the initial CT findings, were then compared between these two groups (Fig. 1). The hematoma volume in the asleep ICH group was significantly larger than that in the awake ICH group (mean ± SD: 32.6 ± 40.6 mL v 16.7 ± 21.0 mL, $P = .0122$). Larger hematomas (≥30 mL) were found in eight of the 19 patients (42.1%) in the asleep ICH group and in 18 of the 103 patients (17.5%) in the awake ICH group. The frequency of these larger hematomas was significantly greater in the asleep ICH group than in the awake ICH group ($P = .0289$).

Table 1. Demographic and clinical characteristics of patients with intracerebral hemorrhage (ICH)

Characteristic	Awake ICH group ($n = 103$)	Asleep ICH group ($n = 19$)	P value
Age (y)	67 ± 11	66 ± 9	0.83
Male	74 (71.8%)	14 (73.7%)	0.87
Prior stroke	15 (14.6%)	2 (10.5%)	1.00
Risk factors			
Hypertension	95 (92.2%)	19 (100%)	0.36
Hyperlipidemia	24 (23.3%)	5 (26.3%)	0.77
Diabetes mellitus	31 (30.1%)	3 (15.8%)	0.27
Cigarette smoking	57 (55.3%)	10 (52.6%)	0.83
Renal function			
Urea nitrogen (mg/dl)	16.2 ± 8.4	14.7 ± 5.7	0.36
Creatinine (mg/dl)	1.0 ± 1.5	0.8 ± 0.5	0.18
Time to arrival (h)	8.9 ± 21.2	12.8 ± 25.7	0.54
Glasgow Coma Scale on admission	14	13	0.14
Blood pressure on admission			
Systolic (mm Hg)	178 ± 32	184 ± 30	0.40
Diastolic (mm Hg)	99 ± 19	105 ± 26	0.39
Heart rate on admission (beats/min)	80 ± 17	81 ± 17	0.77
Location of hemorrhage			
Putamen	34 (33.0%)	8 (42.1%)	0.44
Thalamus	37 (35.9%)	7 (36.8%)	0.94
Lobes	8 (7.8%)	2 (10.5%)	0.65
Cerebellum	9 (8.7%)	1 (5.3%)	1.00
Brainstem	12 (11.7%)	1 (5.3%)	0.68
Multiple	3 (2.9%)	0 (0%)	1.00
Ventricular extension	40 (38.8%)	7 (36.8)	0.87
mRS at 1 month	3	4	0.23
Death within 1 month	5 (4.9%)	4 (21.1%)	0.03

ICH = intracerebral hemorrhage; mRS = modified Rankin Scale.

Values are mean ± SD for age, urea nitrogen, createnine, time to arrival, and blood pressure; median for Glasgow Coma Scale and mRS; the number of patients for the others.

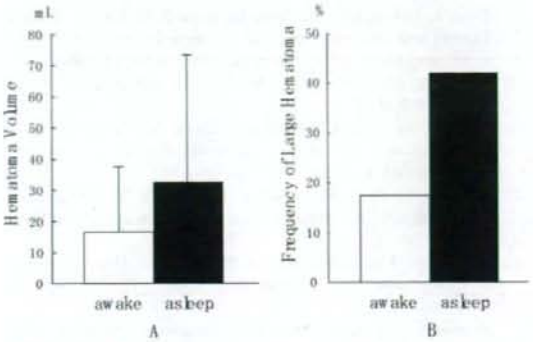

FIG. 1. (**A**) Hematoma volume in the asleep intracebral hemmorrhage (ICH) group is significantly greater than that in the awake ICH group ($P = .0122$, unpaired t test). (**B**) Frequency of large (≥30 mL) hematoma is significantly greater in the asleep ICH group than in the awake ICH group ($P = .0289$, Fisher exact test).

Discussion

It has been speculated that the final triggering mechanisms for the arterial rupture may be caused by an acute increase in the BP that exceeds the tolerance of the vessel wall.[1,6] Generally ICH occurs during the awake period and less frequently during the asleep period.[1] During the awake and active period, the BP may increase concomitantly with exertion or emotional stress, and this sudden BP increase may trigger ICH.[1,6] It is questionable whether a similar BP increase can occur during the asleep period. In 1923, MacWilliam specifically described that the BP may increase suddenly and greatly during the asleep period in patients with heart disease.[7] As later confirmed, such a sudden increase in the BP usually occurs during the transition from non–rapid eye movement (non-REM) sleep to REM sleep, exhibiting phasic surges during REM sleep.[3,8,9] Coccagna et al reported that the increased BP during REM sleep sometimes exceeded the highest values recorded during the awake period in normotensive individuals.[10]

The previous studies of the circadian variation of ICH indicated that the incidence between midnight and 6 AM was 3.0% to 16.9%.[11–18] This wide range of frequency is caused by different study populations and varying diagnostic criteria. Tsementzis et al studied the activity before the onset of ICH in 118 patients and found that 16 patients (13.6%) had ICH while sleeping or upon awakening.[12] Wroe et al reported that the frequency of the onset of primary ICH during sleep was 16.7% (11/66) in a prospective community-based study.[19] In the present study, the frequency of ICH during the asleep period was 14.7%, which was similar to the values reported in the previous articles. Thus, ICH during the asleep period is not as rare as previously thought. The clinical significance of ICH during the asleep period appears to have been excessively underestimated.

To our knowledge, this is the first report describing the clinical features of ICH during the asleep period. Our study indicated that hematoma volume was greater and that the mortality rate at 1 month after the stroke was higher in the asleep ICH group than in the awake ICH group. At the time of ICH development during the asleep period, any witnesses to the ictus event may also be sleepy or drowsy. If symptoms in the asleep ICH group are observable during the awake period, the patients are more likely to notice their own symptoms earlier or their families might discover the stroke episodes earlier. Therefore, ictus during the night-time probably delays awareness of symptom onset. Moreover, the time between the onset of ictus and the arrival to hospital was longer in the asleep ICH group than in the awake ICH group, although the difference between these two groups was not statistically significant. Because the expansion of hematoma commonly occurs in the hyperacute stage,[20] it is speculated that both the delayed detection of symptom onset and the arrival delay, resulted in larger hematoma in the asleep ICH group. The greater volume of the hematoma is reported to be closely linked with the higher mortality rate at 1 month after the stroke.[21,22]

Dyken et al reported that one of four patients with obstructive sleep apnea and ICH developed the stroke during the asleep period.[23] Sleep apnea syndrome (SAS) drastically affects BP during the asleep period. The BP rises appreciably with each apneic episode, in some cases exceeding 200 mm Hg during REM sleep, and then returns back to control values after resumption of normal ventilation.[24,25] Thus, BP shows cyclic elevations during the asleep period. It is reasonable to assume that such phasic surges play a crucial role in the occurrence of ICH during the asleep period. To clarify the exact mechanism of ICH during the asleep period, a prospective follow-up of hypertensive patients using 24-h ambulatory BP measurement and polysomnography needs to be studied in detail in the future.

References

1. Ojemann RG, Mohr JP: Hypertensive brain hemorrhage. Clin Neurosurg 1975;23:220–244.
2. Littler WA, Honour AJ, Carter RD, Sleight P: Sleep and blood pressure. Br Med J 1975;3:346–348.
3. Khatri IM, Freis ED: Hemodynamic changes during sleep. J Appl Physiol 1967;22:867–873.
4. Kazui S, Minematsu K, Yamamoto H, Sawada T, Yamaguchi T: Predisposing factors to enlargement of spontaneous intracerebral hematoma. Stroke 1997;28:2370–2375.
5. Kothari RU, Brott T, Broderick JP, Barsan WG, Sauerbeck LR, Zuccarello M, Khoury J: The ABCs of measuring intracerebral hemorrhage volumes. Stroke 1996;27:1304–1305.
6. Zulch KJ: Pathological aspects of cerebral accidents in arterial hypertension. Acta Neurol Belg 1971;71:196–220.
7. MacWilliam JA: Blood pressure and heart action in sleep and dreams: their relation to haemorrhages angina and sudden death. Br Med J 1923;22:1196–1200.

8. Snyder F, Hobson JA, Morrison DF, Goldfrank F: Changes in respiration, heart rate, and systolic blood pressure in human sleep. J Appl Physiol 1964;19:417–422.
9. Sei H, Morita Y: Why does arterial blood pressure rise actively during REM sleep? J Med Invest 1999;46:11–17.
10. Coccagna G, Mantovani M, Brignani F, Manzini A, Lugaresi E: Arterial pressure changes during spontaneous sleep in man. Electroencephalogr Clin Neurophysiol 1971;31:277–281.
11. Passero S, Reale F, Ciacci G, Zei E: Differing temporal patterns of onset in subgroups of patients with intracerebral hemorrhage. Stroke 2000;31:1538–1544.
12. Tsementzis SA, Gill JS, Hitchcock ER, Gill SK, Beevers DG: Diurnal variation of and activity during the onset of stroke. Neurosurg 1985;17:901–904.
13. Sloan MA, Price TR, Foulkes MA, Marler JR, Mohr JP, Hier DB, Wolf PA, Caplan LR: Circadian rhythmicity of stroke onset: intracerebral and subarachnoid hemorrhage. Stroke 1992;23: 1420–1426.
14. Franke CL, van Swieten JC, van Gijn J: Circadian and seasonal variation in the incidence of intracerebral hemorrhage. Cerebrovasc Dis 1992;2:44–46.
15. Marshall J: Diurnal variation in occurrence of strokes. Stroke 1977; 8:230–231.
16. Gallerani M, Trappella G, Manfredini R, Pasin M, Napolitano M, Migliore A: Acute intracerebral hemorrhage: circadian and circannual patterns of onset. Acta Neurol Scand 1994;89:280–286.
17. Ricci S, Celani MG, Vitali R, La Rosa F, Righetti E, Duca E: Diurnal and seasonal variations in the occurrence of stroke: a community-based study. Neuroepidemiology 1992;11:59–64.
18. Arboix A, Marti-Vilalta JL: Acute stroke and circadian rhythm. Stroke 1990;21:826.
19. Wroe SJ, Sandercock P, Bamford J, Dennis M, Slattery J, Warlow C: Diurnal variation in incidence of stroke: Oxfordshire Community Stroke Project. Br Med J 1992;304:155–157.
20. Kazui S, Naritomi H, Yamamoto H, Sawada T, Yamaguchi T: Enlargement of spontaneous intracerebral hemorrhage: incidence and time course. Stroke 1996;27:1783–1787.
21. Qureshi AI, Tuhrim S, Broderick JP, Batjer HH, Hondo H, Hanley DF: Spontaneous intracerebral hemorrhage. N Engl J Med 2001; 344:1450–1460.
22. Broderick JP, Brott TG, Duldner JE, Tomsick T, Huster G: Volume of intracerebral hemorrhage: a powerful and easy-to-use predictor of 30-day mortality. Stroke 1993;24:987–993.
23. Dyken ME, Somers VK, Yamada T, Ren ZY, Zimmerman MB: Investigating the relationship between stroke and obstructive sleep apnea. Stroke 1996;27:401–407.
24. Klingelhofer J, Hajak G, Sander D, Schulz-Varszegi M, Ruther E, Conrad B: Assessment of intracranial hemodynamics in sleep apnea syndrome. Stroke 1992;23:1427–1433.
25. Tilkian AG, Guilleminault C, Schroeder JS, Lehrman KL, Simmons FB, Dement WC: Hemodynamics in sleep-induced apnea: studies during wakefulness and sleep. Ann Intern Med 1976;85:714–719.

Original Paper

Cerebrovascular Diseases

Cerebrovasc Dis 2006;21:367–371
DOI: 10.1159/000091545

Received: June 21, 2005
Accepted: November 17, 2005
Published online: February 15, 2006

Early CT Findings in Unknown-Onset and Wake-Up Strokes

Kenichi Todo Hiroshi Moriwaki Kozue Saito Makiko Tanaka Hiroshi Oe Hiroaki Naritomi

Cerebrovascular Division, Department of Medicine, National Cardiovascular Center, Osaka, Japan

Key Words
Early CT findings, stroke · Unknown-onset stroke · Wake-up stroke

Abstract
Background: Approximately one quarter of the acute ischemic stroke patients notice the event at awakening. Such patients with stroke at awakening are usually excluded from thrombolysis, since the time of stroke onset cannot be definitely identified. We compared the hyperacute CT findings of awakening stroke patients with those of stroke patients with known onset to assess whether the time of stroke onset is shortly before awakening. ***Methods:*** Subjects were cardioembolic stroke patients who were consecutively admitted to our department within 3 h after the recognition of stroke during the period between January 2000 and March 2003. The patients were classified into three groups: group A with stroke of known onset, group B with stroke at awakening, and group C with stroke of unknown onset due to lack of a witness. The clinical and CT findings in each group were compared. ***Results:*** A total of 81 patients fulfilled the study criteria. There were 46 patients in group A, 17 patients in group B, and 18 patients in group C. There was no significant difference in CT findings between groups A and B. In group C, however, definite hypodense areas were more commonly found than in group A (56 vs. 0%; $p < 0.001$) or in group B (56 vs. 11%; $p = 0.012$). ***Conclusion:*** Based on our CT findings, stroke at awakening seems to be developing shortly before in a large subset of patients, making them potential candidates for acute stroke therapies.

Introduction

Approximately one quarter of acute ischemic stroke patients notice the stroke at awakening [1–3]. Such patients with stroke at awakening are usually excluded from acute stroke treatments, such as thrombolysis with recombinant tissue plasminogen activator, since the time of stroke onset cannot be definitely identified [4]. Barber et al. [5] reported that the major reasons for not receiving thrombolytic therapy included awakening with mild symptoms, erroneous self-judgement for symptomatic improvement, delay caused by transfer from an outlying hospital, and inaccessibility of a treating hospital. Thrombolytic therapy for acute ischemic stroke would be more beneficial, if it were accessible to more patients. There is a possibility that some patients may wake up at the time of stroke onset and may be good candidates for a thrombolytic therapy.

Fink et al. [6] reported that the clinical features and MRI findings of patients who wake up with ischemic symptoms do not differ significantly from those with known onset time. These authors concluded that some

KARGER

Fax +41 61 306 12 34
E-Mail karger@karger.ch
www.karger.com

1015–9770/06/0216–0367$23.50/0

Accessible online at:
www.karger.com/ced

Kenichi Todo, MD
Department of Cardiovascular Medicine
Osaka University Graduate School of Medicine, 2-2 Yamadaoka, Suita
Osaka 565-0871 (Japan)
Tel. +81 6 6879 3634, Fax +81 6 6878 6574, E-Mail ktodo@medone.med.osaka-u.ac.jp

patients who wake up with ischemic symptoms have favorable imaging characteristics for acute stroke therapy. In a clinical situation, however, CT rather than MRI is more widely used before thrombolytic treatment of hyperacute ischemic stroke, because CT is more accessible [7]. To our knowledge, there is no report describing the hyperacute CT findings in detail in patients who wake up with stroke. To verify the hypothesis that a large subset of such stroke patients who wake up with ischemic symptoms may have developed stroke shortly before awakening, we compared the hyperacute CT findings of awakening stroke patients with those of stroke patients with known time of onset and also with those of stroke patients with unknown onset due to the lack of a witness.

Patients and Methods

We retrospectively studied acute cardioembolic stroke patients who were consecutively admitted to our department and underwent CT scanning within 3 h after the recognition of stroke between January 2000 and March 2003. To make the cohort of our study as homogeneous as possible, we included only cardioembolic patients. Included were patients undergoing complete clinical examinations and CT scans within 3 h after recognition of neurological deficits, patients whose follow-up CT and/or MRI showed supratentorial infarct, and cardioembolic stroke patients diagnosed according to the TOAST (Trial of Org 10172 in Acute Stroke Treatment) classification [8]. Patients with infratentorial ischemic stroke and transient ischemic attacks were excluded from the study. Among the 246 acute stroke patients admitted within 3 h of recognition, we excluded 88 patients with hemorrhagic stroke, 17 with infratentorial ischemic stroke, 29 with large-artery atherosclerosis, 12 with small-vessel occlusion, 15 with stroke having another determined etiology, and 4 with stroke of undetermined etiology diagnosed according to the TOAST classification. Consequently, we recruited a total of 81 consecutive cardioembolic stroke patients. 20 of these 81 patients had multiple infarcts or a history of stroke.

Prospectively recorded data for each patient included stroke risk factors, concomitant cardiovascular diseases, circumstances of stroke onset or detection by a witness, time of the last healthy condition, time of stroke recognition, and National Institute of Health Stroke Scale (NIHSS) score [9] on admission. Information about the circumstances of stroke onset was obtained from a witness. Time of stroke recognition was defined as the time when the witness or the patient first noticed focal neurological symptoms.

We classified all the patients into three groups: group A with stroke of known onset with a witness who confirmed that the patient had been healthy within 1 h prior to stroke recognition; group B with stroke recognized by a witness and/or the patient when she/he woke up from sleep, with going-to-bed time being >1 h before awakening, and group C with stroke of unknown onset due to lack of a witness and due to the patient being unable to determine or communicate its onset – last healthy condition >1 h but not more than 24 h before being found.

CT scans were performed in all patients within 3 h after the recognition of stroke. All CT scans were performed without contrast enhancement using an X-Vigor (Toshiba, Tokyo, Japan) machine (120 kV, 170 mA, 10-mm collimation, matrix size 512 × 512, 2- or 3-second scan time). Three experienced stroke specialists retrospectively analyzed CT films on admission in a blinded manner. They knew that the cohort was a hyperacute stroke population. They were aware of the NIHSS score and the side of the affected hemisphere, both informations are usually available in a clinical decision-making situation. They were unaware of other clinical information such as the circumstances of stroke onset and the time of stroke onset. The three independent physicians read the CT films on admission without knowledge of the follow-up CT and/or MRI. These three observers were trained to identify early CT signs. The findings were classified into three categories (1) normal, if the observers found no sign of acute ischemic stroke; (2) early signs, if the observers found an area of slightly decreased attenuation without clear-cut margin, and (3) hypodense, if the observers found a definite hypodense area. Early CT signs included attenuation of the lentiform nucleus and of corticomedullary contrast and loss of the insular ribbon [10]. Other signs of slightly decreased attenuation of the parenchyma without clear-cut margin were judged as early signs. In cases of disagreement in the findings, these three same observers reviewed the CTs together, and a discussion was held until agreement was reached.

The clinical and CT findings in each group were compared. Continuous data are expressed as mean values ± SD. The Mann-Whitney U test was used for comparison of continuous variables, and Fisher's exact test was used for 2 × 2 tables. Statistical significance was set at $p < 0.05$.

Results

A total of 81 patients (54 men and 27 women; mean age 71 years, age range 24–89 years) fulfilled the inclusion criteria. There were 46 stroke patients with known onset time (group A), 17 patients with stroke at awakening (group B), and 18 stroke patients with unknown onset (group C). The baseline clinical characteristics are summarized in table 1. The time from the last healthy condition in group A was significantly shorter than in group B or C ($p < 0.01$), while the time was almost the same in groups B and C. In group C, the longest and the shortest time after the last healthy condition was 10.0 and 3.5 h, respectively. The time from the recognition of stroke did not differ among the three groups. Age, gender, NIHSS score, and side of lesion were the same in the three groups.

The CT findings for the groups are summarized in table 2. There was no significant difference in CT findings between groups A and B. In group C, however, definite hypodense areas were more commonly found than in group A (56 vs. 0%; $p < 0.001$) and in group B (56 vs. 11%; $p = 0.012$).

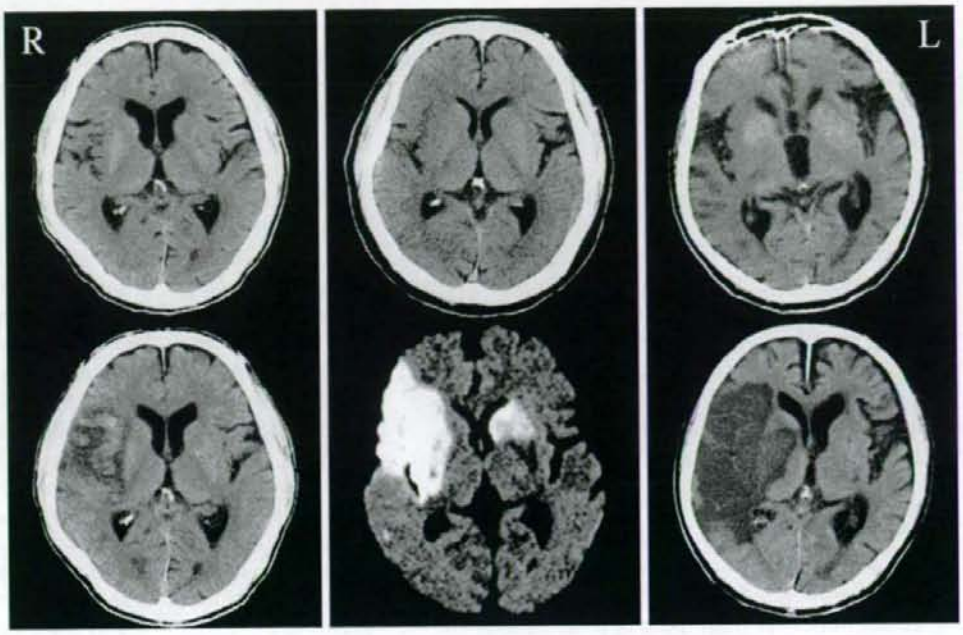

Fig. 1. Hyperacute CT scans (upper) and follow-up CT or MRI scans (lower) of 3 representative patients in group B. Hyperacute CT scans showed no abnormal findings (left), early ischemic signs (middle), and definite hypodense areas (right).

Table 1. Baseline clinical characteristics of the three study groups

	Group A	Group B	Group C
Number of patients	46	17	18
Male/female ratio	30/16	11/6	13/5
Age, years (mean ± 1 SD)	70 ± 13	76 ± 10	75 ± 10
NIHSS score (mean ± 1 SD)	11 ± 7	14 ± 7	13 ± 8
Time from the last healthy condition, h (mean ± 1 SD)	1.7 ± 0.5*	7.5 ± 3.0	5.8 ± 1.6
Time from recognition, h (mean ± 1 SD)	1.7 ± 0.5	1.8 ± 0.5	1.9 ± 0.5
Side of lesion (right/left)	25/21	11/6	11/7

* Time from the last healthy condition was shorter in group A than in group B ($p < 0.01$) or group C ($p < 0.01$).

Table 2. CT findings of the three groups

	Group A (n = 46)	Group B (n = 17)	Group C (n = 18)	p		
				A vs. B	B vs. C	A vs. C
Normal	14 (30%)	4 (22%)	0	0.76	0.10	0.0066
Early signs	32 (70%)	11 (67%)	8 (44%)	0.99	0.31	0.086
Hypodense area	0	2 (11%)	10 (56%)	0.069	0.012	<0.001

In group B, hyperacute CT showed no abnormal findings in 4 patients, early ischemic signs in 11 patients, and definite hypodense signs in the other 2 patients. Representative CT images of group B are shown in figure 1. Stroke was recognized between 00.00 and 06.00 h in 6 of the 17 patients, between 06.01 h and noon in 10 of the 17 patients, and between 18.01 and 00.00 in the remaining group B patient. 8 of the 17 group B patients themselves found ischemic symptoms at awakening. In 6 other patients, family members were the first to become aware of the stroke, when they tried to wake up the patients, noting signs such as consciousness disturbances or motor paralysis. In the remaining 3 patients, the family noticed some unusual behavior of the patients, such as a loud cry, an unusual snore, or a fall resulting in an accident.

Discussion

Our study found that the CT findings within 3 h of stroke recognition in patients who were awakening with stroke did not differ from those in patients with known time of onset, while the CT findings of patients with unknown onset were considerably different from those of the other two groups. Judging from such CT findings, it can be said that stroke may in fact be developing shortly before awakening in a large subset of cardioembolic stroke patients whose stroke is noticed at awakening.

To our knowledge, this is the first report to describe the hyperacute CT findings in detail in patients who wake up with stroke. Recently, Serena et al. [11] compared the clinical characteristics and CT findings in patients with stroke onset at awakening and those with stroke onset while awake who were admitted within 6 h of stroke awareness. These authors reported that there were no relevant differences in the clinical and CT findings between the two groups. However, unlike in our study, they did not identify the precise time of stroke recognition for patients developing stroke at awakening.

The sensitivity of early CT in documenting ischemic changes depends on the duration of the focal cerebral ischemia. Von Kummer et al. [12] reported that parenchymatous low density was identified in 22 of 30 patients (73%) within 3 h of the onset of symptoms and in all 14 patients between 3 and 6 h after onset. The sensitivity of early CT in documenting ischemic changes depends also on the severity of focal cerebral ischemia. Cardioembolic infarcts likely produce more severe tissue damage compared with thrombotic infarcts [13]. On the basis of these reports, to make the cohort of our study as homogeneous as possible, hyperacute CT findings in only cardioembolic patients were compared in this study.

Diagnosing early CT signs is often relatively difficult, as the CT findings may be quite subtle [14]. This difficulty is reflected by the significant interobserver variability in interpreting initial CTs [15, 16]. The positive rate of CT signs varies according to the type of study (retrospective or prospective) and the type of analysis performed (blinded or not to clinical data) [10]. Von Kummer et al. [12] reported that there was a 5% false-positive rate on CT done within 6 h of stroke read without knowledge of the symptoms and signs. In this study, there were no false positives on CT read with knowledge of the NIHSS score and the affected hemisphere. The observers did not identify an old or recent infarct as a new-onset infarct.

Such patients, if transferred rapidly to a hospital after waking up with stroke, may have some salvageable tissue. Instead of noncontrast CT, the ischemic penumbra imaging (by perfusion-weighted/diffusion-weighted MRI, perfusion-weighted CT, xenon CT, or SPECT) would be even more suitable to assess these patients for their potential to benefit from acute stroke treatments. However, there may be time-dependent cellular processes that confer an increasing risk of hemorrhage, such as progressive endothelial cell damage, which are not reflected by any current imaging techniques [6]. Even using currently available MRI techniques, an accurate estimation of a lesion's age is quite difficult [17]. At present, the information that is essential for the initiation of a thrombolytic therapy is an accurate time of stroke onset. Hyperacute therapies for ischemic stroke could have more impact, if they were accessible to the appropriate subset of awakening stroke patients.

The present investigation has the limitation that the study sample included only cardioembolic stroke patients, not representing the average stroke population. If patients with other types of ischemic stroke, such as atherothrombotic or lacunar stroke, were included into the study, completely different results might have been obtained. This should be kept in mind when our results are taken into consideration about stroke treatment in the future. Nevertheless, the present results are considered worth reporting, since ischemic stroke patients who are admitted to stroke care units within 3 h after stroke recognition most likely have cardioembolic stroke, and since the decision to perform or not to perform thrombolytic therapy in cardioembolic stroke has more consequences meaning than in other types of ischemic stroke.

References

1 Elliott WJ: Circadian variation in the timing of stroke onset: a meta-analysis. Stroke 1998; 29:992–996.

2 Lago A, Geffner D, Tembl J, Landete L, Valero C, Baquero M: Circadian variation in acute ischemic stroke: a hospital-based study. Stroke 1998;29:1873–1875.

3 Chaturvedi S, Adams HP Jr, Woolson RF: Circadian variation in ischemic stroke subtypes. Stroke 1999;30:1793–1795.

4 The National Institute of Neurological Disorders and Stroke rt-PA Stroke Study Group: Tissue plasminogen activator for acute ischemic stroke. N Engl J Med 1995;333:1581–1587.

5 Barber PA, Zhang J, Demchuk AM, Hill MD, Buchan AM: Why are stroke patients excluded from TPA therapy? An analysis of patient eligibility. Neurology 2001;56:1015–1020.

6 Fink JN, Kumar S, Horkan C, Linfante I, Selim MH, Caplan LR, Schlaug G: The stroke patient who woke up: clinical and radiological features, including diffusion and perfusion MRI. Stroke 2002;33:988–993.

7 Adams HP Jr, Adams RJ, Brott T, del Zoppo GJ, Furlan A, Goldstein LB, Grubb RL, Higashida R, Kidwell C, Kwiatkowski TG, Marler JR, Hademenos GJ; Stroke Council of the American Stroke Association: Guidelines for the early management of patients with ischemic stroke: a scientific statement from the Stroke Council of the American Stroke Association. Stroke 2003;34:1056–1083.

8 Adams HP Jr, Bendixen BH, Kappelle LJ, Biller J, Love BB, Gordon DL, Marsh EE 3rd: Classification of subtype of acute ischemic stroke: definitions for use in a multicenter clinical trial. TOAST. Trial of Org 10172 in Acute Stroke Treatment. Stroke 1993;24:35–41.

9 Brott T, Adams HP Jr, Olinger CP, Marler JR, Barsan WG, Biller J, Spilker J, Holleran R, Eberle R, Hertzberg V, Walker M: Measurements of acute cerebral infarction: a clinical examination scale. Stroke 1989;20:864–870.

10 Moulin T, Cattin F, Crepin-Leblond T, Tatu L, Chavot D, Piotin M, Viel JF, Rumbach L, Bonneville JF: Early CT signs in acute middle cerebral artery infarction: predictive value for subsequent infarct locations and outcome. Neurology 1996;47:366–375.

11 Serena J, Davalos A, Segura T, Mostacero E, Castillo J: Stroke on awakening: looking for a more relational management. Cerebrovasc Dis 2003;16:128–133.

12 von Kummer R, Nolte PN, Schnittger H, Thron A, Ringelstein EB: Detectability of cerebral hemisphere ischaemic infarcts by CT within 6 h of stroke. Neuroradiology 1996;38: 31–33.

13 Moulin T, Crepin-Leblond T, Chopard JL, Bogousslavsky J: Hemorrhagic infarcts. Eur Neurol 1994;34:64–77.

14 Tomura N, Uemura K, Inugami A, Fujita H, Higano S, Shishido F: Early CT finding in cerebral infarction: obscuration of the lentiform nucleus. Radiology 1988;168:463–467.

15 Grotta JC, Chiu D, Lu M, Patel S, Levine SR, Tilley BC, Brott TG, Haley EC Jr, Lyden PD, Kothari R, Frankel M, Lewandowski CA, Libman R, Kwiatkowski TG, Broderick JP, Marler JR, Corrigan J, Huff S, Mitsias P, Talati S, Tanne D: Agreement and variability in the interpretation of early CT changes in stroke patients qualifying for intravenous rtPA therapy. Stroke 1999;30:1528–1533.

16 Kalafut MA, Schriger DL, Saver JL, Starkman S: Detection of early CT signs of >1/3 middle cerebral artery infarctions: interrater reliability and sensitivity of CT interpretation by physicians involved in acute stroke care. Stroke 2000;31:1667–1671.

17 Schwamm LH, Koroshetz WJ, Sorensen AG, Wang B, Copen WA, Budzik R, Rordorf G, Buonanno FS, Schaefer PW, Gonzalez RG: Time course of lesion development in patients with acute stroke: serial diffusion- and hemodynamic-weighted magnetic resonance imaging. Stroke 1998;29:2268–2276.

Annals of Nuclear Medicine Vol. 20, No. 3, 245–251, 2006

System design and development of a pinhole SPECT system for quantitative functional imaging of small animals

Toshiyuki AOI,*,** Tsutomu ZENIYA,* Hiroshi WATABE,* Hossain M. DELOAR,* Tetsuya MATSUDA** and Hidehiro IIDA*

*Department of Investigative Radiology, National Cardiovascular Center Research Institute
**Department of System Science, Graduate School of Informatics, Kyoto University

Recently, small animal imaging by pinhole SPECT has been widely investigated by several researchers. We developed a pinhole SPECT system specially designed for small animal imaging. The system consists of a rotation unit for a small animal and a SPECT camera attached with a pinhole collimator. In order to acquire complete data of the projections, the system has two orbits with angles of 90° and 45° with respect to the object. In this system, the position of the SPECT camera is kept fixed, and the animal is rotated in order to avoid misalignment of the center of rotation (COR). We implemented a three dimensional OSEM algorithm for the reconstruction of data acquired by the system from both the orbitals. A point source experiment revealed no significant COR misalignment using the proposed system. Experiments with a line phantom clearly indicated that our system succeeded in minimizing the misalignment of the COR. We performed a study with a rat and ^{99m}Tc-HMDP, an agent for bone scan, and demonstrated a dramatic improvement in the spatial resolution and uniformity achieved by our system in comparison with the conventional Feldkamp algorithm with one set of orbital data.

Key words: pinhole SPECT, complete data acquisition, small animal imaging

INTRODUCTION

IN VIVO IMAGING of physiological functions (e.g., the tissue blood flow and receptor binding potentials) in small laboratory animals facilitates the objective assessment of pharmaceutical development and regenerative therapy in pre-clinical trials. Micro positron emission tomography (PET) has been extensively emphasized for achieving high spatial resolution in the imaging of small animals, which approaches 1.0 mm.[1–3] An alternative methodology for small animal imaging is micro single photon emission computed tomography (micro SPECT) in which a camera is fitted with a pinhole collimator.[4–8] Pinhole SPECT has low sensitivity as compared with small animal PET; however, depending on the size of the pinhole, the spatial resolution achieved by pinhole SPECT can exceed that of PET. Unlike PET systems, the pinhole SPECT system does not require a cyclotron for producing radiopharmaceuticals, and it has an excellent cost/performance ratio. Moreover, the half life of radiopharmaceuticals used for pinhole SPECT is relatively longer than that used for PET, which is beneficial in investigating slow pharmacokinetics.

In addition to the lower sensitivity of pinhole SPECT, the existence of image distortion in the axial direction and non-uniform spatial resolution in the reconstructed image for the pinhole SPECT are also areas of concern. One explanation for this non-uniformity is due to incompleteness of data and use of Feldkamp filtered backprojection (FBP) algorithm as an approximate 3D FBP.[9] This non-unifomity can be suppressed by applying statistical reconstruction algorithms such as maximum likelihood expectation maximization (MLEM)[10,11] or ordered subsets expectation maximization (OSEM),[12] but in the periphering of FOV, the

Received June 30, 2005, revision accepted December 13, 2005.

For reprint contact: Toshiyuki Aoi, R.T., Department of Investigative Radiology, National Cardiovascular Center Research Institute, 5–7–1 Fujishiro-dai, Suita, Osaka 565–8565, JAPAN.
E-mail: toshiaoi@ri.ncvc.go.jp

image is blurred.[5,13] This non-uniformity of the image resolution often hampers further quantitative analysis. Tuy showed that in order to obtain a strict three-dimensional (3D) tomogram in cone-beam CT, the following geometric condition should be fulfilled: "all the planes that cross an object cross the axis of the X-ray source."[14,15] Tuy's condition can be adapted to pinhole SPECT. The conventional pinhole SPECT with one circular orbit does not fulfill this condition. Kudo and Saito suggested examples of orbits that can satisfy Tuy's condition: use of two circular orbits, a spiral orbit, or a single circular orbit in conjunction with a straight line.[16–18] By satisfying Tuy's condition, Zeniya et al. demonstrated an improvement in the uniformity of the spatial resolution of pinhole SPECT by using two circular orbits with angles of 90° and 45° with respect to the object.[19] However, they did not present details of a system configuration including hardware and software. In this paper, we focused on the detailed descriptions of system (hardware as well as software) which is able to properly acquire data from two circular orbits.

MATERIALS AND METHODS

System configuration

The misalignment of the center of rotation (COR) could be more critical for data acquisition with two orbits as compared with a single orbital system. Therefore, in the proposed system, the detector and collimator were fixed, and the small animal was rotated. The outline of the system and the data flowchart are shown in Figure 1. This system consists of a rotation unit (RU), rotation unit control board (RU controller), pinhole collimator, and SPECT camera.

Rotation unit (RU)

A small animal was rotated on the RU (Fig. 2), which consisted of a base-board and a rotating stage. The rotating stage was driven by a stepping motor (SGSP-120YAW-θz, Sigma Company, Tokyo, Japan) with a COR accuracy of 20 μm. As shown in Figure 2, the small animal can be fixed in the direction of either 90° or 45°. The axes of the two directions intersect each other, and the distances between the intersection point and each base are equal ($T1 = T2$). In order to perform data acquisition with two circular orbits, the intersection point must coincide with the COR of the pinhole detector, i.e., the line perpendicular to the detector center should cross the intersection point, as shown in Figure 2. An adjustment implement (Fig. 3) was utilized to achieve this. The implement was designed to position a radioactive point source at the COR. Then, the COR was adjusted by acquiring data with the point source for various angle directions.

The rat holder was prepared such that the femoral parts and tail of the rat would lie out of the holder (Fig. 4). It was fabricated from 0.5 mm-thick vinyl chloride.

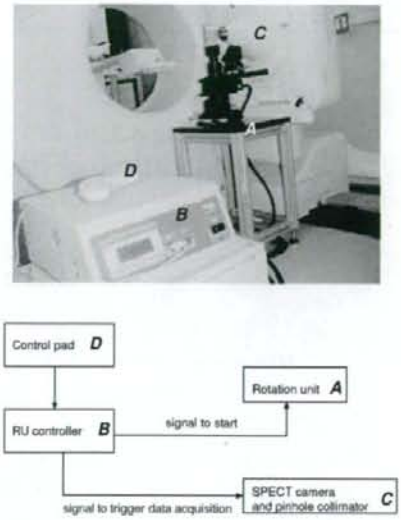

Fig. 1 *Upper:* Overview of the proposed pinhole SPECT system for small animals. *Lower:* Schematic diagram of the system. (A) rotation unit (RU), (B) RU controller, (C) SPECT camera and pinhole collimator, and (D) control pad.

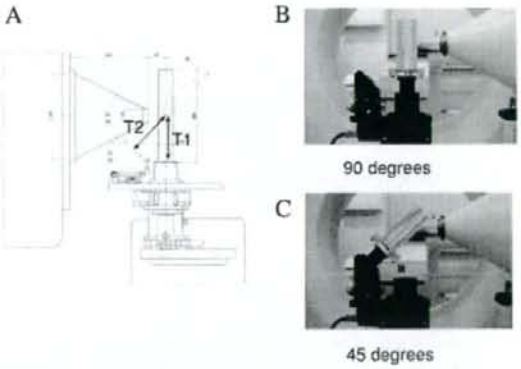

Fig. 2 Cross section of the rotation unit (A) and schematic views of the 90° orbit (B) and 45° orbit (C).

RU controller

In order to control the RU, a general-purpose controller (Mark202, Sigma Company, Tokyo, Japan) was employed. The RU controller could control the starting point of the stepping motor, rotation direction, step angle, and speed of rotation using a control pad. The minimum amount of movements per pulse was 0.01° and the maximum speed of movement was 100°/s.

Pinhole collimator

The pinhole collimator (NDCL709A, Toshiba, Tokyo, Japan) used had a tungsten knife-edge head, which was replaceable. The available hole sizes were 0.25 mm, 0.5

mm, 1 mm, 2 mm, and 4.8 mm. The pinhole had an open angle of 60°, and the distance between the pinhole center and the detector surface was 251 mm. The diameter of the bottom of the collimator was 288 mm.

SPECT camera

A clinically used SPECT camera (GCA-7100A, Toshiba, Tokyo, Japan) with one detector was used. As shown in Figure 1, the camera stayed in one position during data acquisition. The acquired projection data had a matrix of size 128 × 128, and the pixel size 4.3 × 4.3 mm^2.

In order to enable data acquisition with the proposed system, the software installed in GCA-7100A was modified to receive a signal from the RU controller. A signal was sent to the RU to begin rotation with a particular stepping angle. After that rotation, a trigger signal was sent to GCA-7100A to acquire the projection data (See Fig. 1). The above process was repeated until the RU completed 360° rotation.

Image reconstruction

We developed a 3D OSEM algorithm for reconstructing the projection data-set acquired with two different circular orbits.[19] Figure 5 describes the coordinates for the 3D reconstruction with the proposed pinhole SPECT system based on two circular orbits, which are defined as (x, y, z), (x', y', z'), and (x'', y'', z''). The radioactivity concentration of the object is expressed within a fixed (x, y, z) system as $f(x, y, z)$. The second coordinate system (x', y', z') represents the tilt of the (x, y, z) system about the y axis with an oblique angle of ϕ. The third coordinate system (x'', y'', z'') is a rotational coordinate system where (x', y', z') rotates around the z axis with an angle θ. The tilt of (x, y, z) by the angle ϕ produces the following transformations:

$$\begin{pmatrix} x' \\ y' \\ z' \end{pmatrix} = R_1 \begin{pmatrix} x \\ y \\ z \end{pmatrix}, R_1 = \begin{pmatrix} \cos\phi & 0 & \sin\phi \\ 0 & 1 & 0 \\ -\sin\phi & 0 & \cos\phi \end{pmatrix} \quad (1)$$

Similar to Eq. (1), which represents the transformation between the (x, y, z) and (x', y', z') coordinates, the following equation expresses that between the (x, y, z) and (x'', y'', z'') coordinates:

$$\begin{pmatrix} x'' \\ y'' \\ z'' \end{pmatrix} = R_2 \begin{pmatrix} x' \\ y' \\ y' \end{pmatrix} = R_2 R_1 \begin{pmatrix} x \\ y \\ z \end{pmatrix}, R_2 = \begin{pmatrix} \cos\theta & -\sin\theta & 0 \\ \sin\theta & \cos\theta & 0 \\ 0 & 0 & 1 \end{pmatrix} \quad (2)$$

In case of $\phi = 0$, the geometry of the system equals that of conventional pinhole SPECT with one circular orbit.[20,21] Therefore, for reconstruction with an oblique orbit, a procedure similar to conventional pinhole SPECT can be applied using Eq. 2. The source voxel (x_1'', y_1'', z_1'') is projected toward the detector thorough the pinhole collimation of the oblique circular orbit, as shown in Figure 6. We denote the detector plane and a plane parallel to it that includes the source voxel as Plane 1 and Plane 2, respectively. The source point $(t_x, t_z) = (x_1'', z_1'')$ on Plane 2 is the projected point (d_x, d_z) on Plane 1. This relationship can be expressed as

$$d_x = -t_x f_l / a \quad (3)$$
$$d_z = -t_z f_l / a$$

where f_l is the distance between the pinhole and the detector plane (focal length) and a is the distance between the pinhole and the plane parallel to the detector plane that includes the source point. The distance a can be expressed as

$$a = (h_x - x_1') \sin\theta + (h_y - y_1') \cos\theta \quad (4)$$

where $(h_x, h_y, h_z) = (r \sin\theta, r \cos\theta, 0)$ is the pinhole position translated by the rotation θ on the oblique circular orbit with radius of rotation r. We employed the MLEM[10,11] reconstruction algorithm for this pinhole geometry. The MLEM update for a two-orbit system can be expressed as

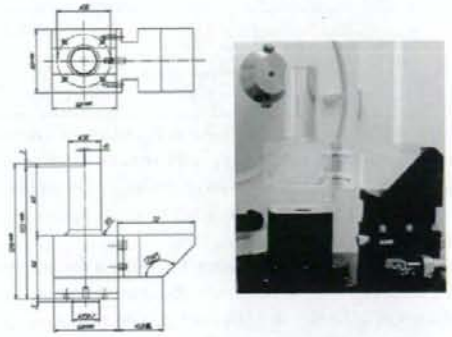

Fig. 3 Adjustment implement to position the point source at the COR of both orbits.

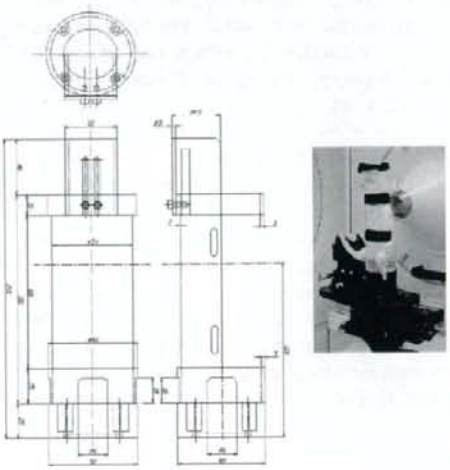

Fig. 4 Rat holder fabricated from 0.5 mm-thick vinyl chloride.

$$\lambda_j^{k+1} = \frac{\lambda_j^k}{\sum_{l=1}^{2}\sum_{i=1}^{n} c_{lij}} \sum_{l=1}^{2}\sum_{i=1}^{n} \frac{y_{li} c_{lij}}{\sum_{j=1}^{m} c_{lij}\, \lambda_j^k} \qquad (5)$$

where, as shown in Figure 5, λ_{jk} is the value of the image voxel j for the k-th iteration, y_{li} is the measured value of the projection pixel i for the l-th orbit, and c_{lij} is the probability of detecting a photon originating from image voxel j at projection pixel i for the l-th orbit.

Here, we used an OS scheme[12] to reduce the number of iterations. Subsets were evenly divided from both orbits for the OS scheme. A 3D voxel-driven projector using bilinear interpolation on the detector plane was employed in both forward- and back-projections. While back-projecting, the projection data from different orbits were transformed into the same coordinate and combined in the reconstructed 3D matrix space. The software was implemented on a 2.4-GHz PC with Xeon CPU and 1 GB of physical memory, running on a Linux operating system (version 2.4.18).

Experiment with a point source

In order to validate whether the projection data from two orbits were correctly acquired, we performed an experiment using a radioactive point source. A point source of about 1.4 mCi/m*l* of $^{99m}TcO_4^-$ was positioned at the COR using the adjustment implement (Fig. 3). A pinhole insert with a diameter of 4.8 mm was employed, and the distance between the pinhole center and point source was 39.5 mm. Projection data were acquired for 120 angular views in steps of 3°. The acquisition time for each step was 15 s. Three images were reconstructed from the projection data with the 90° orbit, 45° orbit, and both the orbits using the 3D OSEM algorithm (2 iterations and 8 subsets). The matrix size of the image was 128 × 128 × 128 and the voxel size was 0.76 × 0.76 × 0.76 mm^3 (zooming factor of 6.35).

Since the point source was positioned at the center of both the 90° and 45° orbits, its positions in the three images should be identical. The 3D position of the point source in each image was estimated by calculating the image center of gravity, and the estimated positions in the three images were compared.

Experiment with a line source

As described above, the misalignment of the COR could be problematic especially for two orbit data acquisition. Thus, in our system, the camera was kept fixed while the target object was rotated. For evaluating the misalignment of the COR for our system as well as the conventional system, experiments were performed using a line source phantom with an inner diameter of 1.14 mm. The phantom was filled with about 4.0 mCi of $^{99m}TcO_4^-$ solution. The phantom was carefully placed at the center in one projection view. First, the pinhole detector was rotated around the phantom with a rotation radius of 9 mm. Next, the phantom was rotated on the rotating stage. In both cases,

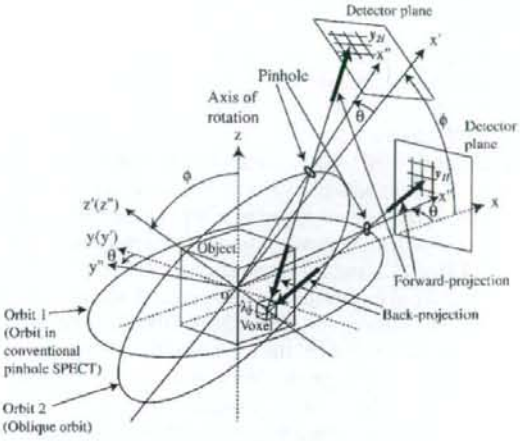

Fig. 5 Coordinate system of oblique circular orbits in pinhole SPECT with two circular orbits.

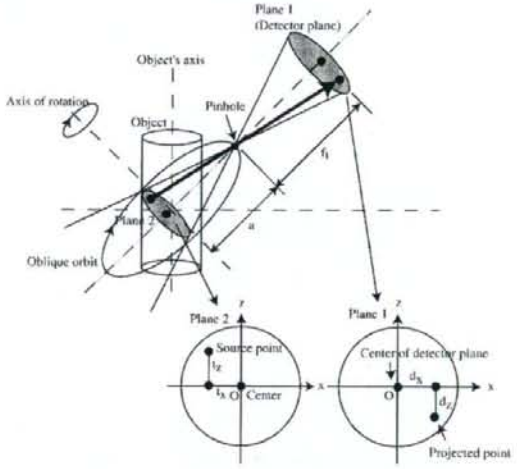

Fig. 6 Pinhole geometry for oblique orbit in pinhole SPECT with two circular orbits.

a pinhole with a diameter of 1 mm was used, and data were acquired from 120 angular views (3°/view). The data by both systems were reconstructed using the 3D OSEM algorithm.

Animal experiment

In order to demonstrate the reconstructed image by our system, a study was performed with a rat (SD rat; body weight: 150 g) and ^{99m}Tc-HMDP, an agent for bone scanning. ^{99m}Tc-HMDP was also accumulated in the bladder of the rat. Therefore, to eliminate the effect of radioactivity in the bladder, both kidneys of the rat were removed before ^{99m}Tc-HMDP (185 MBq/m*l*) was intra-

Table 1 Results of the experiment with a point source. Estimated position of the point source in the image

	x (mm)	y (mm)	z (mm)
90° orbit	0.0505	0.0511	0.0137
45° orbit	0.0464	0.0426	0.0290
both orbits	0.0643	0.0504	0.0165

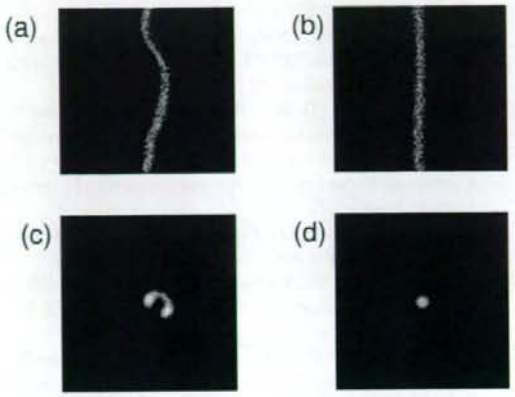

Fig. 7 Results of the experiments with the line source phantom. (a) Sinogram data measured by the conventional system (rotating the camera), (c) image reconstructed by the conventional system, (b) sinogram data measured by the proposed system (rotating the object), and (d) image reconstructed by the proposed system.

venously injected. The rat was set on the rotation unit of 90° orbit and data acquisition using the proposed system was begun 1 h after the injection. The rotation radius was 85 mm, and data were acquired from 120 angular views (3°/view) for 40 min. Subsequently, the rat was set on the rotation unit of the 45° orbit and data were acquired for 40 min. The energy window was 140 keV ± 10%. The diameter of the pinhole insert was 1 mm. The acquired data were sent to the PC for reconstruction using the 3D OSEM algorithm with two iterations and eight subsets. For comparison, the conventional filtered backprojection algorithm (the Feldkamp FBP algorithm)[9] was employed to reconstruct the image using the data acquired from the 90° orbit. No correction for attenuation of photons or scattered rays was made in any of the processes.

RESULTS

Experiment with a point source

Table 1 lists the estimated positions of the point source in the three reconstructed images. These three point-source positions were almost at the center (the distance from the center was 0.083 mm at maximum) and were close in value. This indicates a sufficient accuracy of intersection of the two axes and the pinhole center.

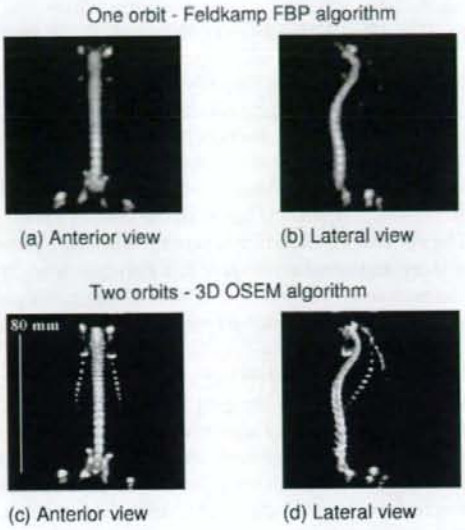

Fig. 8 Representative images of rat bone scintigrams by ^{99m}Tc-HMDP. The images of (a) and (b) were reconstructed using the Feldkamp FBP algorithm with data from the 90° orbit. The images of (c) and (d) were reconstructed using the 3D OSEM with two orbital data. All images were generated by the maximum intensity projection (MIP) method.

Experiment with a line source

Figure 7 shows the results of the experiments with a line source phantom. Misalignment of the COR was clearly observed when the camera was rotated. This results in an artifact on the reconstructed image (Fig. 7 (c)). On the other hand, no obvious artifact was observed when our system was used.

Animal experiment

Figure 8 shows the maximum intensity projection (MIP) images of the rat with ^{99m}Tc-HMDP obtained using the Feldkamp FBP algorithm with one set of orbital data and the 3D OSEM with two orbital data. The artifact of the image was significantly reduced, and a thin rib was clearly observed when data from two orbitals were used.

DISCUSSION

In this paper, we present the pinhole SPECT system for imaging small animals using data from two orbits. In the proposed system, the position of the detector is kept fixed while the target object is rotated.[22] As compared with the conventional system with one orbit, our system requires a more accurate adjustment of the COR. The experiments with the point and line sources indicated that our system achieved sufficient accuracy in adjusting the COR of the two orbits. This result was apparent in the bone scan with a rat. Image distortion and axial blurring observed in the

one orbital system were greatly improved in the proposed system with two orbits.

Metzler et al. proposed the use of a helical scan system in order to acquire complete data by pinhole SPECT.[23] In the helical scan, sensitivity may be hampered when the pinhole moves across the target object. On the other hand, the sensitivity of our system is not affected since the object is positioned at the center of the field-of-view.

The system proposed in this paper is still in the prototype stage, and in order to acquire data from two orbits, the object must be moved from one orbit to the other. We plan to build a system with multiple pinhole detectors in order to increase the sensitivity.

Our final goal is to develop a system that achieves quantitative functional imaging of small animals. Although the image quality achieved by the proposed system has dramatically improved, several issues have yet to be considered for quantification. Penetrated photons at the collimator and photons scattered from the object as well as the collimator will degrade the image quality and quantity.[24] It is also important to consider the sensitivity compensation of the pinhole collimator when reconstructing an image.[25] In order to achieve a quantitative functional image using the proposed system, these issues should be rectified in the future.

CONCLUSION

We developed a pinhole SPECT system for the imaging of small animals. The proposed system consists of two axes so that complete data are acquired. Image uniformity was dramatically improved by our system. This system will provide accurate quantitative information on the biological functions of small animals.

ACKNOWLEDGMENT

This study was financially supported by the Budget for Nuclear Research of the Ministry of Education, Culture, Sports, Science and Technology, based on screening and counseling by the Atomic Energy Commission.

REFERENCES

1. Chatziioannou AF. PET scanner dedicated to molecular imaging of small animal models. *Mol Imaging Biol* 2002; 4: 47–63.
2. Tai YC, Chatziioannou AF, Yang Y, Silverman RW, Meadors K, Siegle S, et al. MicroPET II: design, development and initial performance of an improved microPET scanner for small-animal imaging. *Phys Med Biol* 2003; 48: 1519–1537.
3. Jeavons AP, Chandler RA, Dettmar CAR. A 3D HIDAC-PET camera with submillimetre resolution for imaging small animals. *IEEE Trans Nucl Sci* 1999; 46: 468–473.
4. Weber DA, Ivanovic M, Franceschi D, Strand S-E, Erlandsson K, Franceschi M, et al. Pinhole SPECT: An approach to *in vivo* high resolution SPECT imaging in small laboratory animals. *J Nucl Med* 1994; 35: 342–348.
5. Jaszczak RJ, Li J, Wang H, Zalutsky MR, Coleman RE. Pinhole collimation for ultra-high-resolution small-field-of-view SPECT. *Phys Med Biol* 1994; 39: 425–437.
6. Ishizu, K, Mukai T, Yonekura Y, Pagani M, Fujita T, Magata Y, et al. Ultra-high resolution SPECT system using four pinhole collimators for small animal studies. *J Nucl Med* 1995; 36: 2282–2287.
7. Ogawa K, Kawade T, Nakamura K, Kubo A, Ichihara T. Ultra high resolution SPECT for small animal study. *IEEE Trans Nucl Sci* 1998; 45: 3122–3126.
8. Aoi T, Watabe T, Deloar HM, Ogawa M, Teramoto N, Kudomi N, et al. Absolute quantitation of regional myocardial blood flow of rats using dynamic pinhole SPECT. Conference Record of IEEE Nuclear Science and Medical Imaging Conference 2002.
9. Feldkamp LA, Davis LC, Kress JW. Practical cone beam algorithm. *J Opt Soc Am* 1984: 29: 612–619.
10. Shepp LA, Vardi Y. Maximum likelihood reconstruction for emission tomography. *IEEE Trans Med Imag* 1982; MI-1: 113–122.
11. Lange K, Carson R. EM reconstruction algorithms for emission and transmission tomography. *J Comput Assist Tomogr* 1984; 8: 306–316.
12. Hudson HM, Larkin RS. Accelerated image reconstruction using ordered subsets of projection data. *IEEE Trans Med Imag* 1994; 13: 601–609.
13. Vanhove C, Defrise M, Franken PR, Everaert H, Deconinck F, Bossuyt A. Interest of the ordered subsets expectation maximization (OS-EM) algorithm in pinhole single-photon emission tomography reconstruction: a phantom study. *Eur J Nucl Med* 2000; 27: 140–146.
14. Tuy HK. An inversion formula for cone-beam reconstruction. *SIAM J Appl Math* 1983; 43: 546–552.
15. Grangeat O, Sire P, Guillemaud R, La V. Indirect cone-beam three-dimensional image reconstruction. In: *Contemporary Perspectives in Three-Dimensional Biomedical Imaging*, Roux C, Coatrieux JL (eds), Amsterdam; IOS Press, 1997: 29–52, 343–350.
16. Kudo H, Saito T. Feasible cone beam scanning methods for exact reconstruction in three-dimensional tomography. *J Opt Soc Am A* 1990; 7: 2169–2181.
17. Kudo H, Saito T. Derivation and implementation of a cone-beam reconstruction algorithm for nonplanar orbits. *IEEE Trans Med Imag* 1994; 13: 196–211.
18. Kudo H, Saito T. An extended completeness condition for exact cone-beam reconstruction and its application. Conference Record of IEEE Nuclear Science and Medical Imaging Conference 1994, 1710–1714.
19. Zeniya T, Watabe H, Aoi T, Kim KM, Teramoto N, Hayashi T, et al. A new reconstruction strategy for image improvement in pinhole SPECT. *Eur J Nucl Med Mol Imag* 2004; 31: 1166–1172.
20. Li J, Jaszczak RJ, Greer KL, Coleman RE. A filtered backprojection algorithm for pinhole SPECT with a displaced center-of-rotation. *Phys Med Biol* 1994; 39: 165–176.
21. Li J, Jaszczak RJ, Coleman RE. Maximum likelihood reconstruction for pinhole SPECT with a displaced center-of-rotation. *IEEE Trans Med Imag* 1995; 14: 407–409.

22. Habraken JB, de Bruin K, Shehata M, Booij J, Bennink R, van Eck Smit BL, et al. Evaluation of high-resolution pinhole SPECT using a small rotating animal. *J Nucl Med* 2001; 42: 1863–1869.
23. Metzler SD, Greer KL, Jaszczak RJ. Helical pinhole SPECT for small-animal imaging: A method for addressing sampling completeness. *IEEE Trans Nucl Sci* 2003; 50: 1575–1583.
24. Deloar HM, Watabe H, Aoi T, Iida H. Evaluation of penetration and scattering components in conventional pinhole SPECT: phantom studies using Monte Carlo simulation. *Phys Med Biol* 2003; 48: 1–14.
25. Smith MF, Jaszczak RJ. The effect of gamma ray penetration on angle-dependent sensitivity for pinhole collimation in nuclear medicine. *Med Phys* 1997; 24: 1701–1709.

Technical note

Nuclear Medicine Communications

Comparison of multi-ray and point-spread function based resolution recovery methods in pinhole SPECT reconstruction

Antti Sohlberg[a,b], Hiroshi Watabe[a], Tsutomu Zeniya[a] and Hidehiro Iida[a]

Background and objectives Statistical reconstruction methods allow resolution recovery in tomographic reconstruction. Even though resolution recovery has the potential to improve overall image quality, pinhole SPECT images are still often reconstructed using simplified models of the acquisition geometry in order to reduce reconstruction time. This paper investigates the benefits of two resolution recovery methods, multi-ray and point-spread function based, in pinhole SPECT by comparing them to uncorrected reconstruction.

Methods Resolution recovery was incorporated into ordered subsets expectation maximization reconstruction algorithm. The first of the correction methods used a simple but very fast multiple projection ray approach, whereas the second, much slower, method modelled the acquisition geometry more accurately using the analytical point-spread function of the pinhole collimator. Line source, Jaszczak and contrast phantom studies were performed and used for comparison.

Results Resolution recovery improved resolution, contrast and visual quality of the images when compared to reconstructions without it. The method based on the point-spread function performed slightly better, but was almost 50 times slower than the much simpler multi-ray approach.

Conclusion The multiple projection ray approach is a promising method for very fast and easy resolution recovery in pinhole SPECT. It has a profound effect on image quality and can markedly improve the resolution–sensitivity trade-off. *Nucl Med Commun* 27:823–827 © 2006 Lippincott Williams & Wilkins.

Nuclear Medicine Communications 2006, 27:823–827

Keywords: pinhole SPECT, resolution recovery, statistical reconstruction

[a]National Cardiovascular Center Research Institute, Suita City, Osaka, Japan and [b]Department of Clinical Physiology & Nuclear Medicine, Kuopio University Hospital, Finland.

Correspondence to Dr Antti Sohlberg, National Cardiovascular Center Research Institute, 5-7-1 Fujishiro-dai, Suita City, Osaka, Japan 565-8565.
Tel: +0081 6833 5012 (ext. 2559); fax: +0081 6 6835 5429;
e-mail: antti@ri.ncvc.go.jp

Received 13 February 2006 Accepted 4 May 2006

Introduction

The use of pinhole single photon emission computed tomography (SPECT) in clinical practice has been limited to small and superficial targets such as the thyroid [1] and joints [2] due to the reduced field of view. Recently, there has been renewed interest in pinhole SPECT, because it enables small animal imaging, where a small field of view is not a serious problem [3–7]. The attractiveness of small animal pinhole SPECT arises from the fact that it can be performed without any dedicated hardware using only a conventional gamma camera, whereas small animal PET, for example, requires an imaging device suitable only for laboratory animals [8].

The quality of SPECT is degraded by three main factors: attenuation, scatter and collimator blurring of which attenuation and scatter are less pronounced in small animal pinhole SPECT [9]. The collimator blurring reduces spatial resolution and forces the use of small diameter pinhole apertures at the cost of severely reduced sensitivity, which is the most important drawback of small animal pinhole SPECT. The sensitivity of pinhole SPECT can be increased by using multi-pinhole collimators [10], but this requires modifications to the standard clinical imaging equipment and is not widely applied. One solution to the poor sensitivity problem might be the use of statistical reconstruction methods such as the maximum likelihood expectation maximization (ML-EM) [11] or the ordered subsets expectation maximization (OS-EM) algorithms [12]. ML-EM and OS-EM can partly recover the loss in resolution caused by collimator blurring by incorporating a model of the acquisition geometry into the algorithm and might therefore allow the use of larger diameter pinhole apertures. Recovery of resolution has been shown to improve the quality of conventional SPECT imaging [13,14], but is not yet commonly used in small animal pinhole SPECT.

The biggest problem in incorporating resolution recovery in pinhole SPECT reconstruction is the large increase in computational burden. The calculation of point-spread function (PSF) look-up tables can take hours and might require several gigabytes of storage space. The fast resolution recovery methods such as the slice-to-slice blurring [15] often used in parallel-beam SPECT are not